J Appl Electrochem (2011) 41:1191–1199
DOI 10.1007/s10800-011-0314-z

ORIGINAL PAPER

Electrode kinetics in non-aqueous vanadium acetylacetonate redox flow batteries

Aaron A. Shinkle · Alice E. S. Sleightholme · Levi T. Thompson · Charles W. Monroe

Received: 13 January 2011 / Accepted: 17 April 2011 / Published online: 8 June 2011

Abstract Three electrode materials (glassy carbon, gold, and platinum) were investigated for application in a non-aqueous single-metal redox flow battery based on vanadium (III) acetylacetonate, supported by tetraethylammonium tetrafluoroborate in acetonitrile. Redox couples associated with the one-electron disproportionation of $V(acac)_3$ were observed in voltammetry for each metal tested. An elementary kinetic model was created and used to determine rates for oxidation or reduction of the vanadium complex. The oxidation rates for $V(acac)_3$ were mass-transfer limited on all electrode materials, suggesting reversible kinetics. For the $V(acac)_3$ reduction reaction, exchange-current densities of 1.3, 3.8, and 8.4 A m^{-2} were observed on glassy carbon, platinum, and gold electrodes, respectively.

Keywords Vanadium acetylacetonate · Single-metal redox flow battery · Non-aqueous electrolyte · Electrode · Organic electrochemistry · Energy-storage

1 Introduction

High-capacity, scalable storage technologies are needed to facilitate the integration into the grid of stochastic energy-delivery systems such as solar collectors and wind turbines. Redox flow batteries (RFBs) are promising energy-storage devices, which are currently being used commercially for peak shaving and load leveling worldwide [1, 2]. The two most common commercial RFBs employ zinc–bromine [3] and all-vanadium [4, 5] chemistries, although many other active-metal combinations have been researched, including iron–chromium [6] and bromine–polysulfide [7]. The all-vanadium RFB mitigates irreversible capacity fade associated with electrolyte mixing by using the same active metal in both electrolyte solutions. Commercial RFBs use aqueous electrolytes, which restrict cell potentials within the stability window of water (1.23 V under standard conditions). Since energy density scales linearly with cell potential, non-aqueous solvents—with potential windows as high as 5 V [8] —may be useful for RFBs. Furthermore, water can only be used over a nominal temperature range of 0–100 °C. Changing the solvent could enable the use of RFBs in extreme climates. For example, acetonitrile is a liquid at temperatures between −45 and 82 °C and is suitable for colder climates, while dimethylformamide is a liquid between −61 and 153 °C.

There are several reports of non-aqueous RFBs using ruthenium, uranium, chromium, manganese, and vanadium chemistries [9–15]. Matsuda et al. and Chakrabarti et al. employed ruthenium bipyridine and acetylacetonate complexes in non-aqueous RFBs and observed cell potentials of 2.6 V [9, 10] and 1.6–1.77 V [11], respectively. Uranium beta-diketonates were examined in a single-metal non-aqueous RFB, with measured cell potentials of 1.0–1.2 V depending on the particular ligand chosen [12]. Chromium and manganese acetylacetonate were found to yield cell potentials of 3.4 [13] and 1.1 V [14], respectively. Some of the authors recently observed a cell potential of 2.2 V for the single-electron disproportionation of $V(acac)_3$ [15].

A. A. Shinkle · A. E. S. Sleightholme · L. T. Thompson · C. W. Monroe (✉)
Department of Chemical Engineering, University of Michigan, Ann Arbor 48109-2136, USA
e-mail: cwmonroe@umich.edu

L. T. Thompson
Hydrogen Energy Technology Laboratory, University of Michigan, Ann Arbor 48109-2136, USA

The electrochemistry of vanadium acetylacetonate was examined by Nawi and Kitamura [16, 17], who used cyclic voltammetry to observe equilibrium potentials for various half-reactions. They determined that vanadium acetylacetonate reduction occurs by a one-step reversible mono-electronic reaction. The reactions associated with the disproportionation of $V(acac)_3$ are:

$$[V(acac)_3]^+ + e^- \leftrightarrow [V(acac)_3]^0 \quad (1)$$

$$[V(acac)_3]^0 + e^- \leftrightarrow [V(acac)_3]^- \quad (2)$$

If crossover of the V(IV) (positively charged $[V(acac)_3]^+$) or V(II) (negatively charged $[V(acac)_3]^-$) ionic complexes occurs, charge-efficiency losses are incurred because the disproportionation reaction reverses in the liquid phase, but no regeneration of the electrolyte solutions is required. Both oxidation and reduction of the $V(acac)_3$ complex have been shown to be coulombically reversible, with anodic-to-cathodic peak height ratios near unity during cyclic voltammetry [16].

Ideally, the electrode in a RFB should be inert and participate in the reactions as a reversible source or sink for electrons [18], but such behavior is not always observed in practice. Rychcik et al. investigated the aqueous all-vanadium RFB electrochemistry with glassy-carbon, gold, lead, and iridium-oxide-on-titanium electrodes [18]. They observed that the electrode material significantly affected the oxidation kinetics and stability; lead was even shown to inhibit the desired reaction. Hodes et al. examined the effects of electrode material on the polysulfide redox half-reaction, which could be used in a bromine-polysulfide RFB [19]. Polarization curves for carbon, platinum black, brass, and various transition-metal sulfides (RuS, PbS, and CoS) revealed that the reaction rates for the polysulfide redox half-reaction were dependent on the type of electrode. Hollax et al. [20] and Lopez-Atalaya et al. [21] studied kinetics of an aqueous iron/chromium RFB. Lopez-Atalaya et al. examined gold-on-graphite electrodes and observed a change in peak shape upon the addition of gold particles to the graphite surface.

Linear-sweep voltammetry (LSV) at microelectrodes can be used to quantify the effect of electrode material in terms of reaction rate constants and liquid-phase transport properties associated with interfacial electrochemical processes. Aoki et al. developed a model to determine the current from a linear-sweep voltammogram based on a single, diffusion-limited elementary half-reaction and compared it to experimental results [22]. A model was created by Baur et al. to measure diffusion coefficients for several systems (aqueous ferrocyanide, aqueous ruthenium hexamine, and non-aqueous ferrocene) which matched literature values with less than 5% error [23]. Mirkin et al. created tables to relate the half- and quartile-wave potentials from LSV to kinetic and mass-transfer parameters [24]. All of this previous literature examines single half-reactions, and is consequently not immediately applicable to the non-aqueous vanadium flow battery system. At equilibrium, the non-aqueous vanadium electrolyte contains small concentrations of $V(acac)_3^-$ and $V(acac)_3^+$ associated with the dissociation of $V(acac)_3$ in bulk solution. The presence of all three oxidation states of the complex results in a mixed current at each electrode during charge and discharge. For example, if the potential at an electrode is large and positive, then oxidation of $V(acac)_3$ via reaction 1 will dominate, but $V(acac)_3^-$, which is present in trace amounts in the bulk, will still oxidize to a minor extent via reaction 2. This coupled behavior makes it difficult to apply previous models to the non-aqueous vanadium chemistry.

It is common for coordination complexes to undergo successive one-electron transfers, where sequentially greater or lesser energies are associated with each electron exchanged [25]; several researchers have modeled these systems. Asselt et al. used chronoamperometry and steady-state voltammetry to measure the diffusion coefficients for several palladium complexes at a gold electrode and observed reversible electron-transfer reactions [26]. Norton et al. used the pseudo-steady cyclic voltammetry, along with a known expression for the equilibrium constant, to determine the reaction rate for comproportionation of methyl viologen in acetonitrile [27]. Both of these previous investigations treat the successive reactions separately. The electron-transfer mechanism, including the effects of neutral-species concentration changes, will be discussed for the non-aqueous vanadium chemistry.

This article reports a study of the effect of electrode type on the oxidation and reduction rates of vanadium acetylacetonate in a tetraethylammonium tetrafluoroborate and acetonitrile electrolyte. Three electrode materials (glassy carbon, gold, and platinum) were evaluated using cyclic and linear-sweep voltammetry to determine the coulombic reversibility, kinetic reversibility, and exchange-current density for $V(acac)_3$ oxidation and reduction on each material. All three oxidation states of the vanadium complex are found to be involved in the observed LSV response, leading to mixed currents that complicate data analysis. A model is proposed to account for the simultaneous transport and reaction of the V(II), V(III), and V(IV) active species.

2 Experimental

2.1 Electrolytes

Electrolyte solutions were prepared by dissolving vanadium (III) acetylacetonate, $V(acac)_3$, (97%, Aldrich, US)

and tetrathylammonium (TEA) tetrafluoroborate (99%, Aldrich, US) in anhydrous acetonitrile (99.8%, Aldrich, US). Solutions were prepared and experiments performed in an argon-filled dry box to remove environmental oxygen and water.

2.2 Microelectrodes

Planar disks of glassy carbon, gold, and platinum were used as working electrodes for the voltammetric experiments. The glassy-carbon microelectrode consisted of a 1 mm glassy-carbon rod embedded in PEEK (ALS, Japan). Gold and platinum microelectrodes were produced by flame-sealing a 100 μm diameter gold or platinum wire (99.998%, Alfa Aesar, US) into soda-lime glass, followed by polishing to expose a disk of the material. All electrodes were polished sequentially with 15, 6, and 0.1 μm silicon carbide paper prior to each experiment.

2.3 Cyclic and linear-sweep voltammetry

Cyclic voltammetry (CV) and LSV were performed using an Autolab PGSTAT302N Potentiostat/Galvanostat (Ecochemie, Netherlands) in a standard three-compartment glass cell. A 5 cm^2 graphite plate (Graphite Store, US) was used as the counter electrode. An Ag/Ag^+ (Basi, US) reference electrode was used, containing acetonitrile-solvated 0.01 M silver nitrate (Basi, US, 99%) and 0.1 M tetraethylammonium perchlorate (Alfa Aesar, US, 98%). A bridging reference solution of 0.05 M tetraethylammonium nitrate (Fluka, US, 98%) was used to establish a thermodynamically meaningful working-electrode potential.

Every experiment was performed at the same dimensionless scan rate, $\dot{\omega}$, to ensure that electrodes of different sizes were examined under similar conditions. The dimensionless scan rate, $\dot{\omega}$, is defined as [28]

$$\dot{\omega} = \frac{\dot{v}\, nFr^2}{RTD} \tag{3}$$

where $\dot{v}$ is the scan rate in V s^{-1}, n is the number of electrons transferred ($n = 1$ in all reactions discussed here), F is Faraday's constant (96485 C mol^{-1}), r is the radius of the disk microelectrode, R is the gas constant (8.314 J mol^{-1} K^{-1}), T is the absolute temperature (296 K), and D is the diffusion coefficient of the neutral active species through the support solution. The temperature and diffusion coefficient were considered constant when determining the dimensionless scan rate. The diffusion coefficient used was 3.93×10^{-6} cm s^{-1}, the determination of which is described later in this report. Results were measured after the voltammogram stabilized, typically after 20 cycles. Peak potentials and currents were measured using the Autolab software package, GPES.

3 Experimental results

Figure 1 shows cyclic voltammograms of a 0.01 M $V(acac)_3$ and 0.05 M $TEABF_4$ solution in CH_3CN, with three different working-electrode materials. A low active-species concentration was used to approach ideal solution behavior and does not reflect the maximum solubility of vanadium acetylacetonate in the system. The maximum solubility of vanadium acetylacetonate in acetonitrile has been reported to be 0.59 ± 0.02 M at room temperature [29]. The scan rate was selected to be as slow as possible while retaining definitive redox peaks, $\dot{\omega} = 500$. To normalize the peak currents with respect to mass-transfer limitations, current densities are multiplied by the electrode radii on the ordinate axis. Isolated peak pairs centered around −1.77 and 0.45 V versus Ag/Ag^+ were observed for all electrode materials. These peak locations are consistent with $V(acac)_3$ oxidation and reduction equilibria, as expressed by Eqs. 1 and 2 [16]. It is important to note that the peak at +0.75 V versus Ag/Ag^+ which was reported previously [15] is not observed because most of the vanadyl acetylacetonate has been removed from the solution precursor [29].

Information about the coulombic and kinetic reversibility can be gained by examining CV results as a function of scan rate, shown in Fig. 2. The coulombic reversibility of a redox couple can be determined from its CV by comparing the anodic and cathodic peak heights at several scan rates [28]. Scan rates for Au and Pt were calculated, according to Eq. 3, by multiplying the glassy-carbon scan rate by 100 to account

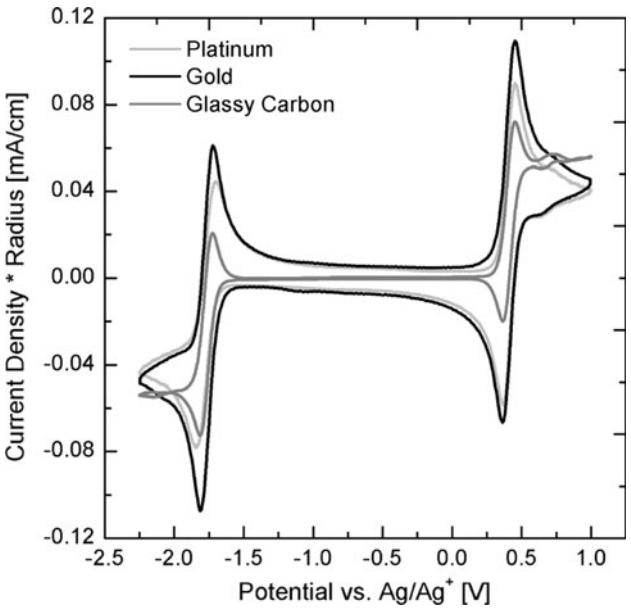

Fig. 1 Cyclic voltammograms ($\dot{\omega}$=500) for glassy carbon, gold, and platinum microelectrodes in 0.01 M $V(III)(acac)_3$, 0.05 M $TEABF_4$ in CH_3CN; measurements performed at 23 °C

for the ten-fold decrease in electrode radius. The peak-height ratios for $V(acac)_3$ reduction, Eq. 2, are 1.00 ± 0.05, 1.03 ± 0.05, and 0.99 ± 0.05 on glassy carbon, gold, and platinum, respectively—each unity within experimental error. The peak-height ratios for $V(acac)_3$ oxidation, half-reaction 1, are 0.98 ± 0.05, 1.05 ± 0.05, and 0.98 ± 0.05 on glassy carbon, gold, and platinum, respectively—again unity within experimental error. Thus, redox reactions were coulombically reversible on all electrodes.

Kinetic reversibility—the relative rates of the anodic and cathodic steps of a given half-reaction—can be evaluated qualitatively using CV by examining the peak separation as a function of scan rate. If the peak separation is constant with respect to scan rate then the system is kinetically reversible (fast) [30]. This indicates that the exchange-current density of the half-reaction is very high, so the overpotential is low and the reaction potential, approximately Nernstian. A range of dimensionless scan rates, $\dot{\omega}$, ranging from 500 to 1,490 were used to determine the peak separation change. The observed change in peak separation over this range of scan rates on glassy carbon, gold and platinum was approximately 20 mV for the $V(acac)_3/V(acac)_3^+$ redox couple (Fig. 2). This small change in peak separation suggests the redox couple is kinetically fast. Peak-separation changes of 20, 70, and 30 mV were observed for the $V(acac)_3/V(acac)_3^-$ redox couple on glassy carbon, platinum, and gold respectively. Glassy carbon has the lowest change in peak separation, however, this observation potentially owes to the larger electrode area used. The small change in peak separation makes it difficult to determine the exchange current using CV methods, justifying the use of LSV, which accounts for the actual reaction mechanism, to better quantify rates.

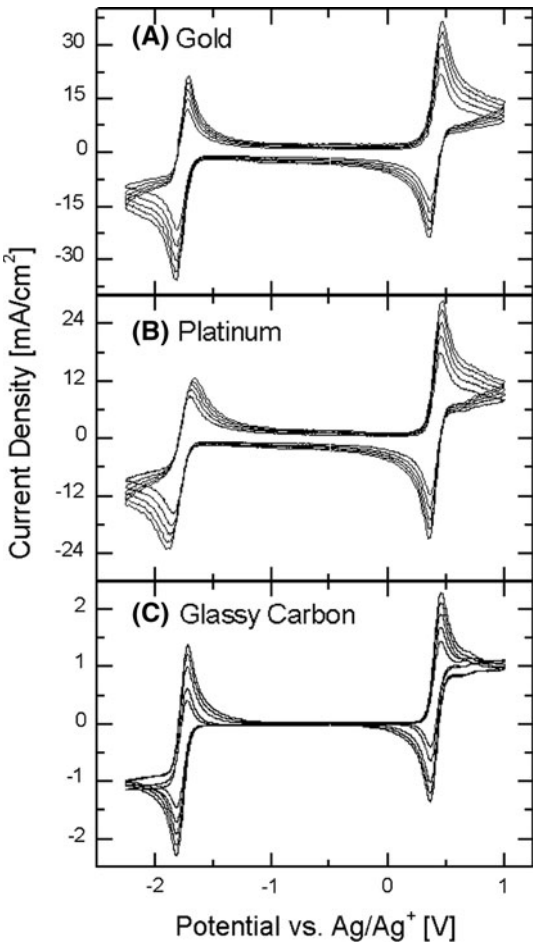

Fig. 2 Cyclic voltammograms ($\dot{\omega}$=500–1490) for **a** gold, **b** platinum, and **c** glassy carbon microelectrodes in 0.01 M $V(III)(acac)_3$, 0.05 M $TEABF_4$ in CH_3CN; measurements performed at 23 °C

4 Mechanistically-based kinetic model

Figures 3 and 4 show LSV results for the $V(acac)_3/V(acac)_3^+$ and $V(acac)_3^-/V(acac)_3$ redox couples, respectively, on each of the three electrode materials. All currents are normalized by the limiting current of the $V(acac)_3/V(acac)_3^+$ redox couple to eliminate electrode-size effects when comparing different disk electrodes. For Figs. 3 and 4, graphs (A)–(C) show data fitted by the model derived below for glassy carbon, gold, and platinum. At least three sets of data are displayed on each plot to illustrate the error associated with the experimental procedure. Graph (D) shows one data set from each electrode material to facilitate comparison among them. A scan rate of 0.3 mV s^{-1} was shown to be suitably slow to achieve pseudo-steady mass transfer for all the electrode sizes. An identical dimensionless scan rate (cf. Eq. 3) was not used in LSV for the largest electrode because bulk concentration changes due to the overall extent of reaction and evaporation of the solvent were found to be significant on that long time scale.

An ideal reversible linear-sweep voltammogram for an elementary half-reaction has a sigmoidal shape centered about zero current at the equilibrium potential [28]. Its anodic and cathodic limiting currents have opposite signs and are proportional to the bulk concentration of oxidized or reduced species, respectively. As the exchange-current density decreases, the sigmoid broadens. In the case where one species concentration is small and kinetics is slow, the linear-sweep voltammogram half-wave potential will be significantly shifted from the equilibrium potential and one of the limiting currents will be very small. The linear-sweep voltammograms in Fig. 3 have half-wave potentials close to the equilibrium potential, suggesting that the reaction rate is fast, but the current has the same sign across the entire wave. In order to rationalize this observation, it is important to note that the electrolyte contains $V(acac)_3^-$, $V(acac)_3$, and $V(acac)_3^+$ in proportions corresponding to the

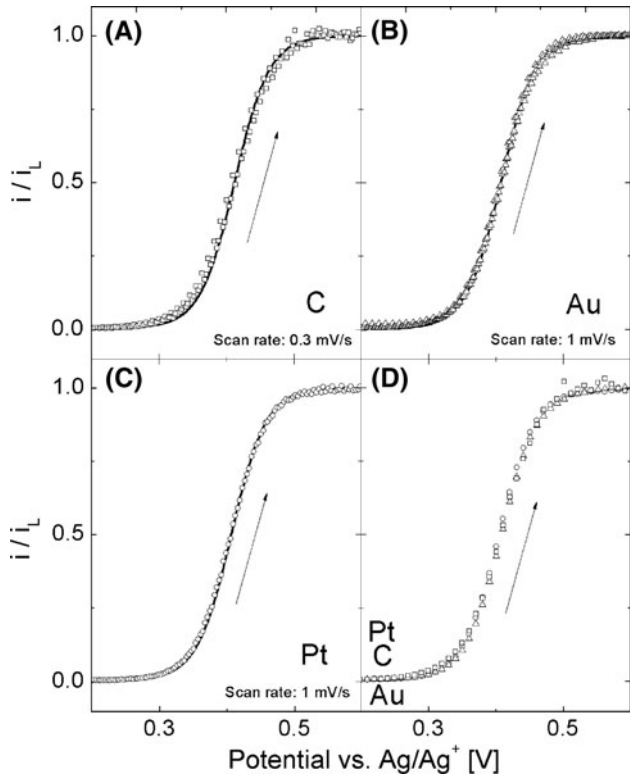

Fig. 3 Linear-sweep voltammograms of the V(III)/V(IV) redox couple at **a** glassy carbon, **b** gold, **c** platinum, and **d** all microelectrodes in 0.01 M V(III)(acac)$_3$ and 0.05 M TEABF$_4$ in CH_3CN. Scan rate 0.3 mV s^{-1} ($\dot{\omega}$=7.4) on glassy carbon and 1 mV s^{-1} ($\dot{\omega}$=0.25) on gold and platinum; measurements performed at 23 °C; arrow indicates direction of change in potential

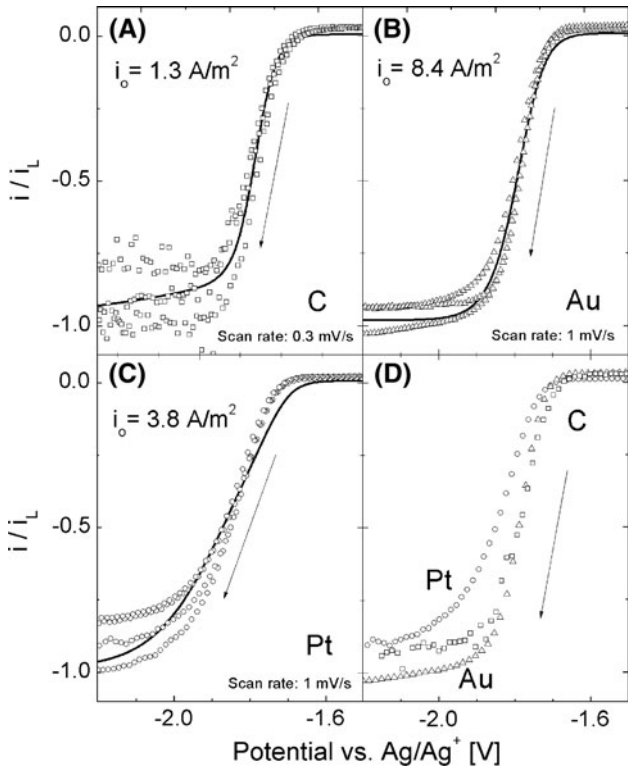

Fig. 4 Linear-sweep voltammograms of the V(II)/V(III) redox couple at **a** glassy carbon **b** gold **c** platinum, and **d** all microelectrodes in 0.01 M V(III)(acac)$_3$ and 0.05 M TEABF$_4$ in CH_3CN. Scan rate 0.3 mV s^{-1} ($\dot{\omega}$=7.4) on glassy carbon and 1 mV s^{-1} ($\dot{\omega}$=0.25) on gold and platinum; measurements performed at 23 °C; arrow indicates direction of change in potential

vanadium (III) acetylacetonate disproportionation equilibrium constant. Since all three species exist in solution, a mixed current is seen from both the oxidation and reduction half-steps of the disproportionation. Thus, when LSV is performed in the potential domain associated with V(acac)$_3$ oxidation, the observed currents stem from the oxidation of both V(acac)$_3$ and V(acac)$_3^-$; when LSV is performed in the V(acac)$_3$ reduction domain, the current reflects reduction of both V(acac)$_3$ and V(acac)$_3^+$.

A second complicating factor is that both reactions 1 and 2 involve V(acac)$_3$; consequently, the currents associated with the two reactions, which both depend on the V(acac)$_3$ concentration, cannot be decoupled [28]. Therefore, a model was created to account for the mixed current generated by two redox reactions.

Both the V(acac)$_3$/V(acac)$_3^+$ and V(acac)$_3^-$/V(acac)$_3$ redox couples are assumed to be elementary. Thus the current density i_n induced by an experimentally controlled potential V can be described in terms of Butler–Volmer kinetic expressions associated with the two simultaneous redox reactions,

$$i_n = i_{0+}^* \left[\frac{c_0}{c_0^*} e^{(1-\beta_+)f(V-E_+^*)} - \frac{c_+}{c_+^*} e^{-\beta_+ f(V-E_+^*)} \right] + i_{0-}^* \left[\frac{c_-}{c_-^*} e^{(1-\beta_-)f(V-E_-^*)} - \frac{c_0}{c_0^*} e^{-\beta_- f(V-E_-^*)} \right] \quad (4)$$

Here c_k is the concentration of active species in state k at the electrode surface and c_k^*, its bulk concentration; subscripts $+$, $-$, and 0 denote properties of the vanadium active complex in its positive (V(IV), [V(acac)$_3$]$^+$), negative (V(II), [V(acac)$_3$]$^-$), and neutral (V(III), [V(acac)$_3$]^0) states, respectively. In the rate expression i_{0k}^* represents the exchange-current density of the half-reaction that converts neutral vanadium to charged species k, β_k is the associated symmetry factor, f equals F/RT, and E_k^* is the equilibrium potential for the half-reaction involving species k measured from CV.

For LSV experiments performed at sufficiently low dimensionless scan rates ($\dot{\omega} < 1$ [28]), the concentration distributions of the various redox states of V(acac)$_3$ can be assumed to be in quasi-steady states within the diffusion layer. Under these circumstances the concentrations of V(acac)$_3^-$ and V(acac)$_3^+$ (c_- and c_+) can be substituted in

favor of their known bulk concentration using the relation for steady-state flux at a disk electrode [31],

$$N_k = 4D_k\left(c_k^* - c_k\right)\ r \tag{5}$$

a material balance at the electrode surface,

$$N_+ + N_- + N_0 = 0 \tag{6}$$

and Faraday's law:

$$i_n = F(N_+ - N_-) \tag{7}$$

where N_k is the molar flux of species k and D_k is the diffusion coefficient of k through the supporting solution.

First Eqs. 4–7 will be used to describe the $V(acac)_3$/$V(acac)_3^+$ redox couple (oxidation of the active complex). Since the equilibrium potentials are very far apart (2.2 V), it is assumed that the current component associated with the $V(acac)_3$/$V(acac)_3^-$ reaction is constant and at the reaction's limiting current. The resulting equation can be simplified by assuming the potential is far away from that of the $V(acac)_3$/$V(acac)_3^-$ reaction, implying $f(V - E_-^*) \gg 1$ and $c_-/c_-^* = 0$. The resulting equation relates the observed current to both dimensionless permeabilities and the exchange-current density of the positive reaction.

$$\frac{i_n}{i_L} = \frac{i_{0+}^*\left[\phi_+(1+2\phi_-)e^{(1-\beta_+)f\left(V-E_+^*\right)} + (\phi_- - \phi_+)e^{-\beta_+ f(V-E_+^*)}\right]}{\phi_+ i_L + i_{0+}^*\left[\phi_+ e^{(1-\beta_+)f\left(V-E_+^*\right)} + e^{-\beta_+ f(V-E_+^*)}\right]} \tag{8}$$

where

$$\phi_+ = \frac{D_+ c_+^*}{D_0 c_0^*} \quad \text{and} \quad \phi_- = \frac{D_- c_-^*}{D_0 c_0^*} \tag{9}$$

also

$$i_L = 4nFD_0 c_0^* r \tag{10}$$

The anodic and cathodic limiting currents for reaction 1 can be identified from Eq. 8 by examining the expression in the limits $V - E_- \to \infty$ and $V - E_- \to -\infty$ to yield

$$\begin{aligned} \frac{i_{L,a}^+}{i_L} &= \lim_{V-E_+^*\to\infty}\frac{i_n}{i_L} = (1+2\phi_-) \text{ and} \\ \frac{i_{L,c}^+}{i_L} &= \lim_{V-E_+^*\to-\infty}\frac{i_n}{i_L} = \frac{\phi_+ + \phi_-}{1+2\phi_-} \end{aligned} \tag{11}$$

During LSV the anodic limiting current is reached when voltages are far positive of the equilibrium potential for $V(acac)_3$ oxidation.

The dimensionless permeabilities of the oxidized and reduced active species through the liquid phase, ϕ_+ and ϕ_-, are defined by Eq. 9. Qualitatively they can be thought of as mobilities of charged active species relative to the neutral active-species mobility. To determine the values of ϕ_+ and ϕ_-, Eq. 8 can be examined in the limit that the exchange current density i_{0+}^* is very large compared to i_L, yielding a mass-transfer limited expression:

$$\frac{i_n}{i_L} = \frac{(\phi_- - \phi_+) + \phi_+(1+2\phi_-)e^{f\left(V-E_+^*\right)}}{1+\phi_+ e^{f\left(V-E_+^*\right)}} \tag{12}$$

In terms of the chemistry being studied here, this assumption implies that there is a minimal kinetic overpotential associated with neutral-vanadium oxidation. This approximation is consistent with the CV experiments discussed earlier, which showed near constant peak separation with respect to scan rate for the $V(acac)_3$/$V(acac)_3^+$ redox couple in CV on all three electrodes (Fig. 2). This observation can be rationalized by Marcus theory, which associates low kinetic overpotentials (high electron transfer rates) with correspondingly low reorganization energy of the reactants and products as well as the electronic structure of the electrode materials [32, 33]. The data for all electrode materials were fit well by this mass-transfer-limited model and were indistinguishable when overlaid. Therefore, $V(acac)_3$ oxidation likely occurs by a mass-transfer-limited elementary electron transfer mechanism on all the electrode materials studied here.

The dimensionless permeabilities in Eq. 9 can be defined in terms of experimental values, which are easily extracted from the data by adding a single measurement of the current density at the equilibrium potential of the $V(acac)_3$/$V(acac)_3^+$ redox half-reaction, $i_n(E_+^*)$, to eliminate i_L. The relations

$$\phi_+ = \frac{i_n\left(E_+^*\right) - i_{L,c}^+}{i_{L,a}^+ - i_n(E_+^*)} \quad \text{and} \quad \phi_- = \frac{i_n\left(E_+^*\right)(i_{L,a}^+ - i_{L,c}^+)}{[i_{L,a}^+ - i_n(E_+^*)](i_{L,a}^+ - 2i_{L,c}^+)} \tag{13}$$

were determined by evaluating Eq. 12 at the equilibrium potential and in the limit of large negative voltages. Here $i_{L,c}^+$ is the cathodic limiting current of the neutral-vanadium reduction half-reaction (the limiting current reached at very negative voltages); and $i_{L,a}^+$ is the anodic limiting current of the neutral-vanadium reduction half-reaction.

Dimensionless permeabilities, ϕ_+ and ϕ_-, were determined by applying the mass-transfer-limited rate expression for oxidative LSV sweeps, and found to be 1.25 ± 0.11 and 1.27 ± 0.12, respectively. The accuracy of the permeabilities was checked by predicting the limiting current of $V(acac)_3$ reduction based on the permeabilities determined using results from the $V(acac)_3$ oxidation. The reduction limiting currents were predicted within 7%—less than the inherent measurement error in the permeabilities. The dimensionless permeabilities are expected to be identical across systems with different electrode materials, since they are solution characteristics. However, it is surprising that both ϕ_+ and ϕ_- are of order 1 because the neutral and charged vanadium complexes are expected to have very different concentrations. Deviations from this

expected characteristic may owe to large differences in the diffusion coefficients or activities of the charged complex compared to the neutral species. They may also owe to the neglect of ionic migration [34].

The dimensionless permeability can be used to evaluate the active-species diffusion coefficient. The diffusion coefficient of $V(acac)_3$ in the supporting electrolytic solution can be derived from Eqs. 5 and 8 evaluated at the equilibrium potential,

$$D_0 = \frac{\left|i^+_{L,a}\right|}{4nFc^*_0 r(1+2\phi_-)} \tag{14}$$

The limiting current, $\left|i^+_{L,a}\right|$, and permeability, ϕ_-, are determined from the experiments shown in Fig. 3. Error in the microelectrode radius and solution concentration increases the uncertainty of the resulting diffusion coefficient. The diffusion coefficient for $V(acac)_3$ in $TEABF_4$-supported CH_3CN was found to be $3.93 \times 10^{-6} \pm 7.2 \times 10^{-7}$ cm^2 s^{-1}, which is approximately 1.5 times the value found by Liu et al. [15] using the Randles–Sevcik method. This difference could be caused by a deviation in the vanadium acetylacetonate concentration from the expected value due to the neglect of vanadyl acetylacetonate formation [29] in the report by Liu et al.

A similar strategy to the one detailed above can be used to describe the neutral-vanadium-complex reduction. When deriving the expression for the reduction current, the assumption of very fast kinetics is no longer valid because the equilibrium potential for the oxidation is close to the onset potential observed in LSV (Fig. 4) and a visible increase of peak separation with scan rate is seen in the CV results (Fig. 2). First, Eqs. 4–7 were used to describe the $V(acac)_3$/$V(acac)_3^-$ redox couple (reduction of the active complex). Since the equilibrium potentials are very far apart (2.2 V), it is assumed that the current component associated with the $V(acac)_3$/$V(acac)_3^+$ reaction is constant at its limiting current. The resulting equation can be simplified by assuming the potential is far away from that of the $V(acac)_3$/$V(acac)_3^+$ reaction, implying that $f(E^*_+ - V) \gg 1$ and $c_+/c^*_+ = 0$. The resulting equation relates the observed current to both dimensionless permeabilities (determined from the positive reaction) and the exchange-current density of the negative reaction.

$$\frac{i_n}{i_L} = \frac{i^*_{0-}\left[(\phi_- - \phi_+)e^{(1-\beta_-)f\left(V-E^*_-\right)} - \phi_-\left(1+2\phi_+\right)e^{-\beta_- f(V-E^*_-)}\right]}{\phi_- i_L + i^*_{0-}\left[e^{(1-\beta_-)f\left(V-E^*_-\right)} + \phi_- e^{-\beta_- f(V-E^*_-)}\right]} \tag{15}$$

The anodic limiting current of half-reaction 2 can be related to the parameter i_L by examining Eq. 15 in the limit $V - E_- \to -\infty$ to yield

$$i_L = \frac{1}{(1+2\phi_-)} i^+_{L,a}. \tag{16}$$

The kinetics of the $V(acac)_3^-$/$V(acac)_3$ redox couple is therefore described by the following equation:

$$\frac{i_n}{\left|i^+_{L,a}\right|} = \frac{\frac{i^*_{0-}}{\left|i^+_{L,a}\right|}\left[(\phi_- - \phi_+)e^{(1-\beta_-)f\left(V-E^*_-\right)} - \phi_-\left(1+2\phi_+\right)e^{-\beta_- f(V-E^*_-)}\right]}{\phi_- + \frac{i^*_{0-}}{\left|i^+_{L,a}\right|}(1+2\phi_-)\left[e^{(1-\beta_-)f\left(V-E^*_-\right)} + \phi_- e^{-\beta_- f(V-E^*_-)}\right]} \tag{17}$$

The current–density parameter i_L and mobilities ϕ_+ and ϕ_- were determined from the experimental data for the $V(acac)_3$/$V(acac)_3^+$ redox couple (Eq. 13). Using transport parameters from the $V(acac)_3$/$V(acac)_3^+$ redox couple to fit the $V(acac)_3^-$/$V(acac)_3$ redox couple adds confidence to the validity of the data-fitting strategy.

Graphs (A)–(C) on Fig. 4 show model fits alongside the data, which were used to calculate exchange-current densities for $V(acac)_3$ reduction. The model current was fit to data by using $i^*_{0-}/i^+_{L,a}$ and β_- as fit parameters with a nonlinear curve fitting program (OriginLab OriginPro 8). Exchange currents were normalized by the anodic limiting currents to facilitate convergence during curve fitting. Prior to performing this analysis, the data were shifted such that the anodic limiting current matched the model prediction. This had to be done to subtract out any current associated with residual dissolved oxygen in the acetonitrile, which is observed at -1.25 V versus Ag/Ag^+ [29]. Shifting the curve is reasonable since neither of these reactants is involved in the reactions of interest [28]. All the data are fit well by Eq. 17, consistent with the assumption that the electron transfers are elementary.

The exchange current for the $V(acac)_3^-$/$V(acac)_3$ redox couple is expected to be comparable to or smaller than i_L since the kinetics is relatively slow. The best-fit values of $i^*_{0-}/i^+_{L,a}$ were 1.5, 0.09, and 0.22 for glassy carbon, platinum, and gold, respectively. These results correlate well with the relative rates of reaction, estimated by the slope and onset potential, observed from Fig. 4 graph **d** as well as peak separations from Fig. 2. Since the glassy-carbon electrode has a ten-fold larger radius, the glassy carbon exchange-current density is smallest. Measured values of exchange-current densities for the three electrode materials are shown in Table 1. The $V(acac)_3^-$/$V(acac)_3$ couple exhibits exchange-current densities of 1.3, 3.8, and 8.4 A m^{-2} on glassy carbon, platinum, and gold, respectively. All of the exchange-current densities are of the same order of magnitude, suggesting that this reaction proceeds through a similar pathway on all of the electrode materials. The peak-separation measurements in CV suggested that the exchange-current density would be smallest on platinum. However, the peak shape also varies according to the values of reaction parameters such as symmetry factors

[24]; the neglect of these may make qualitative conclusions from CV uncertain. Since the electrode materials all yield exchange-current densities of the same order, and gold and platinum cost significantly more than carbon, it would be more practical to use glassy carbon as the electrode material. The exchange current of a carbon electrode can be increased by using high-surface-area carbon.

Despite the differences in active-complex structure and metal valence states between the non-aqueous and aqueous vanadium RFB chemistries, values for the half-reaction exchange-current densities can provide meaningful comparisons of the kinetic overpotential losses between the two systems. In the aqueous system, the largest overpotential comes from the positive electrode: the V(IV)/V(V) redox couple has the lowest exchange-current density, which indicates the slowest reaction kinetics. Zhong and Skyllas-Kazacos reported that the exchange-current density (based on geometric surface area) for the V(IV)/V(V) redox couple at a carbon electrode was 2.47 A m^{-2} [35]. The largest kinetic overpotential in the non-aqueous system comes from the reaction that takes place at the negative electrode, the $V(acac)_3^-/V(acac)_3$ redox couple. On glassy carbon, this reaction has a slightly lower exchange-current density than the aqueous V(IV)/V(V) couple; on gold and platinum, the V(II)/V(III) reaction exchange current densities are higher. Also, the non-aqueous $V(acac)_3/V(acac)_3^+$ redox couple is reversible (immeasurably large exchange-current density)—it is significantly faster than any electrode process in the aqueous all-vanadium flow battery. It is also worth noting that even the lowest exchange-current densities reported by Zhong and Skyllas-Kazacos are relatively high in light of the peak separation shown in CV during the same study [35]. Measured exchange-current densities in the aqueous system may be artificially large, owing to differences between the superficial and electrochemical surface areas of the electrodes used.

The exchange current is the key parameter that determines the kinetic overpotential of a RFB. As the exchange current increases, the RFB kinetic overpotential decreases. An expression for linear kinetics (in the limit that applied voltage V is near the equilibrium voltage E_-) can be used to approximate the kinetic overpotential in a RFB assuming small overpotential [28],

$$\Delta E = \frac{RT}{nF}\frac{i}{i_0} \tag{18}$$

The authors reported a constant-current (1.4 A m^{-2} charge current) charge/discharge curve in an H-cell configuration with carbon electrodes and observed charge voltages of up to 2.9 V (0.7 V of overpotential) [15]. Under those conditions, using Eq. 18, the total kinetic overpotential is estimated to be 31 mV. Therefore, even with carbon electrodes, in this case the kinetics was sufficiently fast that it only contributed $\sim$4% of the total overpotential observed. The main criterion when choosing an electrode material for the non-aqueous vanadium RFB system is the electrode stability because the rates are similar, and high, on several electrode materials.

Table 1 Symmetry factor and exchange-current density for the V(II)/V(III) redox couple at glassy carbon, gold, and platinum electrodes in 0.01 M $V(III)(acac)_3$, 0.05 M $TEABF_4$ in CH_3CN; measurements performed at 23 °C

Electrode material	Symmetry factor (β)	Exchange-current density
Glassy carbon	0.079 ± 0.007	1.3 A m^{-2}
Platinum	0.278 ± 0.003	3.8 A m^{-2}
Gold	0.567 ± 0.008	8.4 A m^{-2}

5 Conclusions

To determine the effect of electrode material on the electrochemistry of the vanadium acetylacetonate/acetonitrile redox-flow-battery system, a mechanistic model was developed. Cyclic voltammetry showed peak-height ratios near unity for all redox couples and electrode materials within experimental error. For oxidation of $V(acac)_3$, the change in peak separation was approximately 20 mV on all electrode materials, while the change in peak separation for the reduction of $V(acac)_3$ was up to 70 mV on platinum. This suggests that the oxidation of $V(acac)_3$ is quasi-equilibrated, whereas its reduction exhibits slower rates.

Linear-sweep voltammetry was used to examine the redox kinetics of $V(acac)_3$ by fitting a two-elementary-step reaction mechanism to the data. The electrode material does not affect the $V(acac)_3/V(acac)_3^+$ redox reaction, for which the electron transfer is very fast. The $V(acac)_3^-/V(acac)_3$ couple has exchange-current densities of 1.3, 3.8, and 8.4 A m^{-2} on glassy carbon, platinum, and gold, respectively. The exchange-current densities have similar magnitude, suggesting a similar electron-transfer mechanism on all three electrode materials. The diffusion coefficient of $V(acac)_3$ was determined based on model parameters and was consistent across all electrode materials, supporting the model's validity. The improvement in reaction rates by using gold or platinum is sufficiently small that it can be overcome by using high-surface-area carbon electrodes.

Acknowledgments The authors acknowledge financial support from the Advanced Energy for Transportation Technology Program and the Hydrogen Energy Technology Laboratory.

References

1. ZBB Energy Corporation (2008) Available via DIALOG. www.zbbenergy.com Cited 15 Dec 2010
2. Prudent Energy (2009) Available via DIALOG. www.pdenergy.com Cited 15 Dec 2010
3. Barnartt S, Forejt DA (1964) J Electrochem Soc 111:1201
4. Sum E, Rychcik M, Skyllas-Kazacos M (1985) J Power Sources 16:85
5. Sum E, Skyllas-Kazacos M (1985) J Power Sources 15:179
6. Hagedorn NH, Thaller LH (1981) J Power Sources 8:227
7. Remick RJ (1984) US Patent 4485154
8. Zoski C (2007) Handbook of electrochemistry. Elsevier, Amsterdam
9. Matsuda Y, Takasu Y, Morita M, Tanaka K, Okada M, Matsumura-Inoue T (1985) Denki Kagaku 53:632
10. Matsuda Y, Tanaka K, Okada M, Takasu Y, Morita M, Matsumura-Inoue T (1988) J Appl Electrochem 18:909
11. Chakrabarti MH, Dryfe RAW, Roberts EPL (2007) Electrochim Acta 52:2189
12. Yamamura T, Shiokawa Y, Yamana H, Moriyama H (2002) Electrochim Acta 48:43
13. Liu Q, Shinkle AA, Li Y, Monroe CW, Thompson LT, Sleightholme AES (2010) Electrochem Comm 12:1634
14. Sleightholme AES, Shinkle AA, Liu Q, Li Y, Monroe CW, Thompson LT (2011) J Power Sources 196:5742
15. Liu Q, Sleightholme AES, Shinkle AA, Li Y, Thompson LT (2009) Electrochem Comm 11:2312
16. Nawi MA, Riechel TL (1981) Inorg Chem 20:1974
17. Kitamura M, Yamashita K, Imai H (1976) Bull Chem Soc Jpn 49:97
18. Rychcik M, Skyllas-Kazacos M (1987) J Power Sources 19:45
19. Hodes G, Manassen J, Cahen D (1980) J Electrochem Soc 127:544
20. Hollax E, Cheng SH (1985) Carbon 23:655
21. Lopez-Atalaya M, Codina G, Perez JR, Vazquez JL, Aldaz A, Climent MA (1991) J Power Sources 35:225
22. Aoki K, Akimoto KT, Matsuda HJ (1984) Electroanal Chem 171:219
23. Baur JE, Wightman MR (1991) J Electroanal Chem 305:73
24. Mirkin MV, Bard AJ (1992) Anal Chem 64:2293
25. Evans DH, Lehmann MW (1999) Acta Chem Scand 53:765
26. Asselt R, Elsevier CJ, Amatore C, Jutand A (1997) Organometallic 16:317
27. Norton JD, White HS (1992) J Electroanal Chem 325:341
28. Bard AJ, Faulkner LR (2001) Electrochemical methods—fundamentals and applications. Wiley, New York
29. Shinkle AA, Sleightholme AES, Griffith LD, Thompson LT, Monroe CW. J Power Sources Accepted 2010. doi: 10.1016/j.jpowsour.2010.12.096
30. Nicholson RS, Shain I (1965) Anal Chem 37:1351
31. Newman J (1970) J Electrochem Soc 17:198
32. Marcus RA (1963) J Phys Chem 67:853
33. Fisher AC (1996) Electrode Dynamics. Oxford, UK
34. Newman J, Thomas-Alyea K (2004) Electrochem Syst. Wiley-Interscience, Hoboken
35. Zhong S, Skyllas-Kazacos M (1992) J Power Sources 39:1